2466–2478 Nucleic Acids Research, 2013, Vol. 41, No. 4 Published online 8 January 2013
doi:10.1093/nar/gks1364

Unwinding of primer-templates by archaeal family-B DNA polymerases in response to template-strand uracil

Tomas T. Richardson[1], Xiaohua Wu[2,3], Brian J. Keith[1], Pauline Heslop[1], Anita C. Jones[2,3] and Bernard A. Connolly[1,*]

[1]Institute of Cell and Molecular Biosciences (ICaMB), The University of Newcastle, Newcastle upon Tyne NE2 4HH, UK, [2]EaStCHEM School of Chemistry, The University of Edinburgh, West Mains Road, Edinburgh EH9 3JJ, UK and [3]Collaborative Optical Spectroscopy Micromanipulation and Imaging Centre (COSMIC), The University of Edinburgh, West Mains Road, Edinburgh EH9 3JJ, UK

Received November 12, 2012; Revised December 5, 2012; Accepted December 6, 2012

ABSTRACT

Archaeal family-B DNA polymerases bind tightly to deaminated bases and stall replication on encountering uracil in template strands, four bases ahead of the primer-template junction. Should the polymerase progress further towards the uracil, for example, to position uracil only two bases in front of the junction, 3′–5′ proof-reading exonuclease activity becomes stimulated, trimming the primer and re-setting uracil to the +4 position. Uracil sensing prevents copying of the deaminated base and permanent mutation in 50% of the progeny. This publication uses both steady-state and time-resolved 2-aminopurine fluorescence to show pronounced unwinding of primer-templates with *Pyrococcus furiosus* (*Pfu*) polymerase–DNA complexes containing uracil at +2; much less strand separation is seen with uracil at +4. DNA unwinding has long been recognized as necessary for proof-reading exonuclease activity. The roles of M247 and Y261, amino acids suggested by structural studies to play a role in primer-template unwinding, have been probed. M247 appears to be unimportant, but 2-aminopurine fluorescence measurements show that Y261 plays a role in primer-template strand separation. Y261 is also required for full exonuclease activity and contributes to the fidelity of the polymerase.

INTRODUCTION

Archaeal family-B DNA polymerases, e.g. the enzymes from *Pyrococcus furiosus* (*Pfu*-Pol) or *Thermococcus gorgonarius* (*Tgo*-Pol), specifically recognize uracil and hypoxanthine, stalling replication on encountering these bases (1–8). A pocket, situated in the polymerase N-terminal domain, interacts with uracil and hypoxanthine using a combination of hydrogen bonds and steric factors to exclude canonical DNA bases, resulting in 100- to 300-fold tighter binding of deaminated base–containing DNA (3–5,8). Stalling is most pronounced with uracil/hypoxanthine four bases (+4) ahead of the primer-template junction (1,2), and DNA with deaminated bases at +4 shows the highest affinity for the polymerase (3). However, primer-templates that contain uracil at +1, +2 and +3 also interact well (3), and for several years, it was unclear how the polymerase could accommodate these different orientations. Several observations have begun to resolve this dilemma. When uracil is located at +4, polymerase activity is strongly inhibited, and the 3′–5′ proof-reading exonuclease slightly reduced. Should the enzyme incorporate additional dNTPs, and therefore, progress towards the deaminated base (e.g. placing uracil at +2), proof-reading exonuclease activity is stimulated (7). This trims back the elongating primer and re-sets uracil to +4, preventing the polymerase extending beyond the deaminated base. It is thought that stalling serves to protect against the inappropriate copying of deaminated bases and the introduction of mutations into the genome (1,2). The increase in exonuclease activity serves as an additional safeguard, demonstrated by the observation that exo$^-$ mutants of the polymerase are better able to replicate beyond uracil than the wild type (7). The polymerase and exonuclease domains of DNA polymerases are well separated, and unwinding of the primer to expose a short single-stranded region is required to position the 3′-terminal base of the primer in the exonuclease active site (9–13). Our group proposed that if the polymerase approaches nearer than four bases to uracil, the primer starts to unravel, giving a short single-stranded region at its 3′ end (7). Such separation

*To whom correspondence should be addressed. Tel: +44 1912 227371; Fax: +44 1912 227424; Email: bernard.connolly@newcastle.ac.uk

explains why primer-templates with uracil at +1, +2 and +3 are still capable of interacting strongly with the polymerase. After binding, an appropriate degree of DNA denaturation creates an actual separation of four bases between the last base pair in the primer-template and the deaminated base. Additionally, the formation of a single-stranded region in the primer accounts for its rapid trimming by the proof-reading exonuclease. A recent crystal structure of *Tgo*-Pol, bound to a primer-template mimic containing hypoxanthine in the +2 position, supported the prediction of unwinding (8). The last two bases at the 3′ end of the primer were single stranded and directed towards the exonuclease active site, resulting in a four-base separation between hypoxanthine and the primer-template junction (Figure 1A).

In family-B DNA polymerases, a β-hairpin motif, comprising two anti-parallel β-strands joined by a loop, critically influences the choice between primer strand extension (catalysed by the polymerase active site) and degradation (carried out by the proof-reading exonuclease centre). Most studied are the viral (bacteriophage) T4 and RB69 family-B polymerases, and structural, kinetic, spectroscopic and mutagenesis data originally suggested that the β-hairpin may actively separate primer and template strands (12–15). A recent study proposed that this motif is responsible for tight binding of DNA as the mismatched primer unwinds from the template strand (16). The structure of *Tgo*-Pol, bound to a hypoxanthine-containing primer-template mimic, showed the β-hairpin in the vicinity of the primer-template junction (Figure 1A), suggesting the motif may be important in the decision between polymerization and proof-reading exonucleolysis. The denatured single-stranded primer was located on one side of the β-hairpin, in the exonuclease channel, with the template found on the other side in the direction of the deaminated base–binding pocket. This structure also highlighted two amino acids, which may be important in tightly binding the partially denatured DNA and/or actively separating primer-template bases and preventing their re-annealing. Arginine 247, an amino acid in the β-hairpin, formed a stacking interaction with one of the newly single-stranded template bases, while tyrosine 261 was positioned between the melted primer-template bases (Figure 1B). As expected, an earlier *Tgo*-Pol structure, using a primer-template mimic with uracil at +4, showed no separation of the primer and template strands (5).

The proposal that archaeal DNA polymerases unwind primer-template strands on approaching uracil or hypoxanthine was initially based on kinetic studies (7) and confirmed by X-ray crystallography (8). Strand separation is common with DNA polymerases but usually takes place with DNA containing mismatched bases, allowing removal of incorrectly incorporated dNMPs. The denaturation of fully Watson–Crick base-paired substrates by archaeal polymerases is, therefore, unusual and merits further investigation, particularly to ensure that the X-ray structure has not fortuitously captured a conformational variant that is rare in solution. The base analogue 2-aminopurine (AP) has long been used as a probe of DNA structure, distortion and dynamics owing to its useful fluorescence properties. The fluorescence of AP (excitation: ~315 nm, emission: ~360 nm) is strongly quenched by base-stacking interactions when it is present in double-stranded DNA (17–19). Oligodeoxynucleotides containing AP have been used to study DNA distortion with a number of enzymes including viral DNA polymerases, with emphasis on the role of the β-hairpin motif in proof reading (15,20,21). Other investigations have focussed on RNA polymerase (22), uracil-DNA-glycosylase (23), DNA methyltransferases (24–26) and

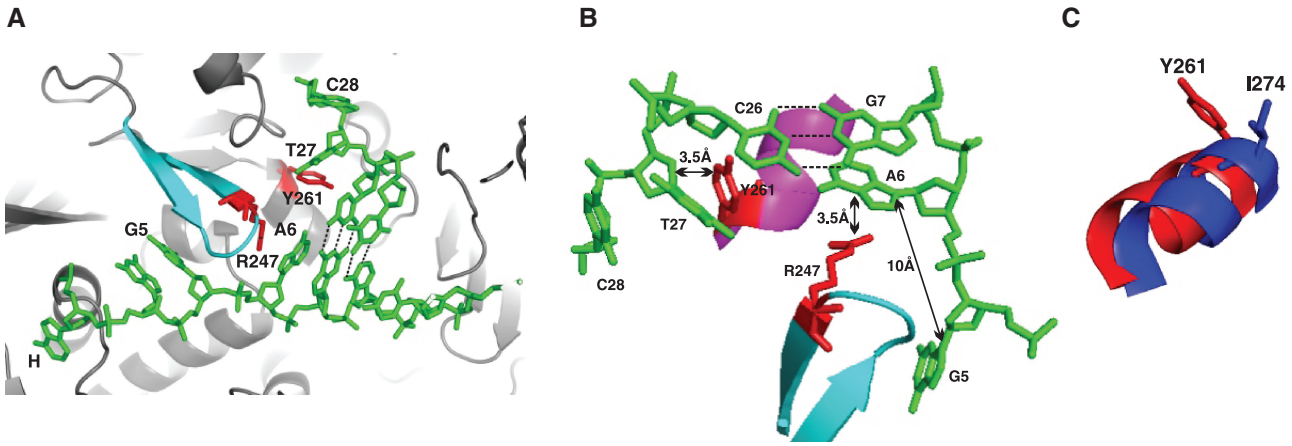

Figure 1. (**A**) Structure of the DNA separation region of *Tgo*-Pol bound to a primer-template mimic containing hypoxanthine at the +2 position (8). The two bases at the extreme 3′ end of the primer, C28 and T27, are single stranded and not base paired with their template partners, G5 and A6, respectively. Thus, the base pairs nearest to the 3′ end of the primer are C26–G7 and T25–A8 (shown with hatched lines indicating Watson–Crick hydrogen bonds rather than being individually labelled). The position of hypoxanthine (H), which is buried in the deaminated base–binding pocket, is also shown. The β-hairpin motif is shown in cyan. Tyr261 and Arg247 are shown in red. The numbering used for the bases is taken from reference 8. (**B**) Interaction of *Tgo*-Pol Y261 and R247 with DNA. C26 and G7 are base paired, but the primer bases T27 and C28 are single stranded and unwound from their complementary template bases A6 and G5. Y261 (red) is located on an α-helix (magenta) ~3.5 Å from T27. R247 (red) is located on the β-hairpin motif (cyan) ~3.5 Å from A6. The N9 atoms of the neighbouring bases A6 and G5 are ~10 Å apart. (**C**) Superimposition of *Tgo*-Pol Y261 (red) with RB69 I274 (blue). Both amino acids are located on the same face of an α-helix. Both structures are taken from editing complexes: *Tgo*-Pol (PDB ID, 2xhb) (8) and RB69-Pol (PDB ID 1clq) (12).

endonuclease V (27). In this publication, steady-state and time-resolved fluorescence of AP has been used to elucidate details of the separation of primer-templates by *Pfu*-Pol. These investigations have been combined with measurements of the exonucleolysis of AP-containing primers. X-ray structural data (8) implied key roles for the archaeal DNA polymerase amino acids at positions 247 (methionine in *Pfu*-Pol, rather than the arginine found with *Tgo*-Pol) and 261 (tyrosine for both *Pfu*- and *Tgo*-Pols) in denaturing primer-templates (Figure 1B). The role and importance of these two amino acids have been further probed using site-directed mutagenesis in conjunction with AP fluorescence and exonuclease assays. Overall, the results further contribute to understanding of deaminated base recognition by these polymerases.

MATERIALS AND METHODS

Protein purification and mutagenesis

Wild-type *Pfu*-Pol and variants lacking either 3′–5′ proofreading exonuclease activity (D215A) or deaminated base recognition (V93Q) were purified as reported previously (28,29). The amino acids methionine 247 and tyrosine 261 were changed to alanine using a QuickChange® site-directed mutagenesis kit (Agilent-Stratagene, Stockport) with Velocity™ DNA polymerase (Bioline, London, UK). The mutated genes were completely sequenced to ensure the presence of the desired mutation and an absence of changes elsewhere. The *Pfu*-Pol mutants M247A, Y261A and the double variant M247A/Y261A were purified in the same manner as the wild-type enzyme. Sodium dodecyl sulphate–polyacrylamide gel electrophoresis with Coomassie blue staining indicated a purity of >95% for all the polymerases used in this publication.

DNA synthesis

All oligodeoxynucleotides were prepared in-house by standard phosphoramidite chemistry and purified by high-pressure liquid chromatography (30,31). The phosphoramidites of AP, fluorescein (6-FAM) and hexachlorofluorescein (HEX) were purchased from Glen Research Corporation (Stirling, VI, USA).

Binding of DNA to *Pfu*-Pol

The dissociation constants (K_D) describing the interaction of *Pfu*-Pol (wild type and the mutants detailed in the results section) with DNA were determined using fluorescence anisotropy with the HEX-labelled primer-templates (3,4) described in Table 1. Spectra were measured in 1-ml volumes at 25°C using two buffers: (i) 10 mM HEPES-NaOH (pH 7.5), 100 mM NaCl, 1 mM ethylenediaminetetraacetic acid (EDTA) [used previously (3,4) and allowing comparison with earlier work] and (ii) 20 mM Tris–HCl (pH 8.5), 20 mM KCl (the buffer used for AP fluorescence measurements). DNA was used at a concentration of 1 nM, and the polymerase from 1 to 50 nM (for uracil-containing DNA) and 10 to 800 nM (for control DNA lacking uracil and for all measurements with *Pfu*-Pol V93Q).

AP steady-state fluorescence

Steady-state fluorescence measurements were performed using the T (control), U+2 and U+4 primer-templates shown in Table 1, both free in solution and bound to *Pfu*-Pol. Fluorescence emission spectra were measured in a 100-µl volume (1-cm path length) quartz cuvette using 2 µM primer-template (consisting of 2 µM AP-containing primer and 4 µM template; native polyacrylamide gel electrophoresis (15%) confirmed that all the AP-containing primers were bound to the template under these conditions) in 20 mM Tris–HCl (pH 8.5) and 20 mM KCl along with either no added divalent metal ion or 2 mM $CaCl_2$ or 2 mM $MgCl_2$. When complexes were to be measured, 8 µM enzyme was added. Contaminating divalent metal ions were removed by adding Chelex resin (Chelex 100 resin, analytical grade, 100–200 mesh, Bio-Rad) to the Tris–KCl buffer and stock solutions of both polymerase and primer-templates for at least 10 h before experimentation. The quartz cuvettes were soaked in 0.1 M EDTA, pH 7.5, and extensively washed with Chelex resin–treated water before use. Fluorescence spectra were collected at 25°C using either an SLM-Aminco or a Cary Eclipse fluorescence spectrophotometer (Varian, Crawley, West Sussex, UK). Spectra were recorded between 340 and 400 nm using an excitation wavelength of 315 nm. With free primer-templates, the spectrum found with buffer alone was subtracted to principally remove the water Raman band. With protein–DNA complexes, a more complex correction needed to be applied:

$$\text{Corrected(Pol-DNA)spectrum} = (\text{Pol-DNA})_{315} - (\text{Pol}_{315} \times (\text{Pol-DNA})_{280}/\text{Pol}_{280})$$

where Pol and (Pol-DNA) are spectra measured with the polymerase alone and for a polymerase–DNA complex, respectively. The subscripts 315 and 280 represent fluorescence spectra measured at these excitation wavelengths. The 280 ratio measures protein fluorescence with and without bound DNA and corrects for the observed drop in protein fluorescence on interaction with nucleic acids, a value of ~0.65 being observed.

Time-resolved AP fluorescence

Measurements of the time-resolved fluorescence of the U+2 and U+4 primer-templates were carried out using conditions (buffers, temperature, DNA and enzyme concentrations) identical to those described for the steady-state measurements. Fluorescence decays were acquired by time-correlated single-photon counting using a Ti-Sapphire femtosecond laser system as excitation source (25,26). The excitation wavelength was 315 nm, with pulses of ~200 fs at 4.75 MHz repetition rate. The instrument response was ~85 ps full width at half maximum, and the fluorescence spectral bandwidth was 10 nm. Decays were collected at three emission wavelengths (365, 380 and 395 nm) and fitted to the function:

$$I(t) = B + \sum_i A_i e^{\frac{-t}{\tau_i}}$$

Table 1. Oligodeoxynucleotides used in this study

Oligodeoxynucleotide (abbreviation)	Oligodeoxynucleotide sequence[a]
T Primer-template (T)	5′-GGGGATCCTCTAGAGTCGACCTGCAGGGC(AP)A-3′ 3′-CCCCTAGGAGATCTCAGCTGGACGTCCCG T TCTTTCGAACAGAGG-5′
U+2 Primer-template (U+2)	5′-GGGGATCCTCTAGAGTCGACCTGCAGGGC(AP)A-3′ 3′-CCCCTAGGAGATCTCAGCTGGACGTCCCG T TCUTTCGAACAGAGG-5′
U+4 Primer-template (U+4)	5′-GGGGATCCTCTAGAGTCGACCTGCAGGGC(AP)A-3′ 3′-CCCCTAGGAGATCTCAGCTGGACGTCCCG T TCTTUCGAACAGAGG-5′

[a]The primer-templates T, U+2 and U+4 were used in AP fluorescence measurements. In each case, 2-aminopurine (AP, shown underlined) is situated one base in from the 3′ end of the primer strand and paired with thymidine. When present, template-strand uracil (U, also shown underlined) is located either two or four bases in front of the primer-template junction (U+2 and U+4, respectively). The primer-templates were also used to measure the dissociation constants (K_D) and 3′–5′ proof-reading exonuclease rates with *Pfu*-Pol B. For K_D determination, HEX was present at the 5′ end of the template. When exonuclease rates were evaluated, 6-FAM was present at the 5′ end of the primer.

where $I(t)$ is the intensity at time t, A_i is the fractional amplitude, τ_i is the fluorescence lifetime of the i-th decay component and B is the background level (dark count of the detector). The three decays, at the different emission wavelength, were analysed globally, i.e. they were fitted simultaneously with lifetimes, τ_i, as common parameters. Quality of fits was assessed by the χ^2 parameter (typically a value <1.2 indicates an acceptable fit) and the randomness of residuals. All the decay curves required four exponential components to give a satisfactory fit, as observed in previous studies (25,26).

Exonuclease assays

Exonuclease assays were performed using the 6-FAM–labelled DNA substrates (10 nM) given in Table 1. Reactions were carried out at 30°C in 400 µl of 20 mM Tris–HCl (pH 8.5), 20 mM KCl, 2 mM $MgCl_2$, 10 nM primer-template and 500 nM *Pfu*-Pol, the polymerase being added last to initiate the reaction. At appropriate times, 40-µl aliquots were withdrawn and quenched with an equal volume of stop buffer (95% formamide, 10 mM EDTA, 10 mM NaOH, 0.1% orange G dye) and 1 µl of a 100 µM solution of 'competitor DNA' (an exact complement of the template strand but lacking fluorescein). The samples were denatured by heating to 95°C for 5 min, and then rapidly cooled on ice. The excess of 'competitor DNA' prevents re-hybridization of the fluorescein primer to the template and ensures that all the fluorescein primers, and products derived from it, remain single stranded during analysis (7). Twenty microlitres of the mixture was loaded for each time point, and the products resulting from exonuclease activity resolved using 17% denaturing polyacrylamide gels. Gels were analysed using a Typhoon scanner (GE Healthcare), and the amount of material present in each product band determined using ImageQuant software (GE Healthcare). Data were fitted to the equation for a first-order reaction (% substrate remaining = $100e^{-kt}$ + offset; k = rate constant, t = time) using GraFit (Erithacus Software, London, UK), allowing determination of rate constants.

Fidelity of *Pfu*-Pol

The fidelities of wild-type, M247A and Y261A *Pfu*-Pol (exo^+) were determined using pSJ2, a *lacZα* gene indicator plasmid, suitable for measuring DNA polymerase accuracy (32). The gapped derivative of pSJ2 (1 nM) was fully extended using *Pfu*-Pol (100 nM) in 20 mM Tris (pH 8.0), 10 mM KCl, 10 mM $(NH_4)_2SO_4$, 2 mM $MgCl_2$, 0.1% (v/v) Triton X-100, 2 µg bovine serum albumin and 250 µM of each of the four dNTPs. Extension was carried out at 70°C for 30 min, and after this time, the mixture was used to transform *E. coli* TOP10 cells, plated on LB agar (containing X-gal, IPTG and ampicillin) and then scored for blue/white colonies as given (32). The conversion of blue/white colony ratios to mutation frequency and error rate has also been previously described (32).

RESULTS AND DISCUSSION

Binding of *Pfu*-Pol to primer-templates

Determining the AP fluorescence of polymerase–DNA complexes requires complete binding of the nucleic acid. Substrate saturation requires a polymerase concentration at least 10 times the K_D describing the interaction, as well as an excess over DNA. *Pfu*-Pol binds tightly to uracil-containing DNA, with low/sub-nanomolar K_D values (2–4). Much weaker affinity is observed for DNA lacking uracil, and in many experiments, the processivity factor PCNA was required to ensure full binding of DNA (7,29). Furthermore, this study makes use of several *Pfu*-Pol mutants, which may bind DNA with lesser affinity than the wild type. Therefore, dissociation constants characterizing the binding between the primer-templates used in this study (Table 1) and *Pfu*-Pol (wild type and relevant mutants) have been determined.

In a previous study, a K_D of 270 nM was measured for a primer-template similar to the T control used in this publication, requiring a polymerase concentration of at least 3 µM for full DNA binding (3). Fortunately, binding was stronger in the buffer used for AP fluorescence measurements and rate determinations, with a K_D of 32 nM being found for interaction of the T primer-template with *Pfu*-Pol (Figure 2A and Table 2).

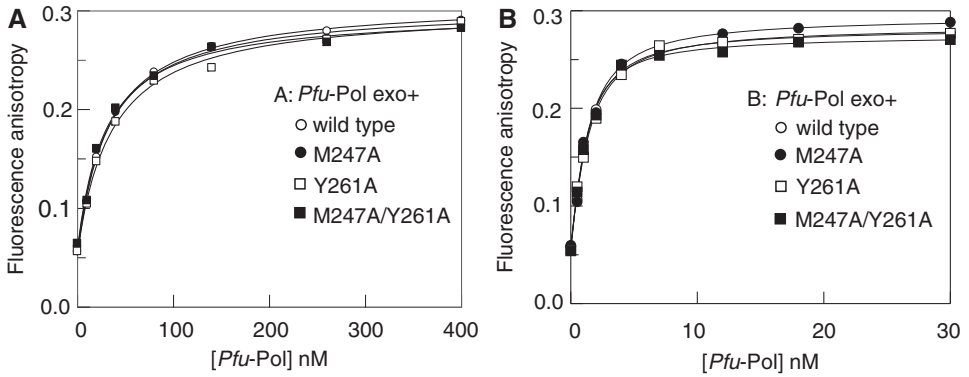

Figure 2. Binding of *Pfu*-Pol B to DNA. Interaction of *Pfu*-Pol exo$^+$ (wild type, M247A, Y261A and M247A/Y261A) with (**A**) control primer-template that lacks uracil (T primer-template given in Table 1) and (**B**) single-stranded uracil-containing oligodeoxynucleotide (the template component alone of the U+2 primer-template given in Table 1). Titrations were carried out in 20 mM KCl (Table 2) using 1 nM oligodeoxynucleotide, and the *Pfu*-Pol levels shown on the graphs. The K_D values describing the binding equilibrium were determined by fluorescence anisotropy as described (3,4,37). K_D values are summarized in Table 2.

Table 2. Binding constants for *Pfu*-Pol B (wild type and mutants) to uracil-containing DNA[a]

Pfu-Pol	K_D values (nM) for *Pfu*-Pol binding to primer-templates at two salt concentrations[b]				
	Primer-template T (KCl)[c]	Primer-template U+4 (NaCl)	Primer-template U+2 (NaCl)	Single stranded U DNA (NaCl)[c]	Single stranded U DNA (KCl)
Wild type exo$^+$	32 ± 4	0.45	3.6	4.2 ± 0.20	0.78
Wild type exo$^-$[d]	ND	0.65	3.8	4.5 ± 0.25	0.88
M247A exo$^+$	31 ± 5	0.58	3.1	4.9 ± 0.35	0.88
M247A exo$^-$	ND	0.72	3.7	4.2 ± 0.45	1.1
Y261A exo$^+$	35 ± 4	0.54	2.9	4.6 ± 0.30	0.89
Y261A exo$^-$	ND	0.64	3.9	4.7 ± 0.28	0.95
M247A/Y261A exo$^+$	29 ± 3	0.48	3.5	4.9 ± 0.45	0.67
M247A/Y261A exo$^-$	ND	0.58	3.4	4.7 ± 0.36	1.0
V93Q exo$^+$[c]	41 ± 3	37 ± 4	28 ± 3	ND	ND

[a]The primer-templates used are given in Table 1. The uracil-containing single-stranded DNA used was the HEX-containing template used to produce the U+2 primer-template.
[b]The salt concentrations used were as follows:
NaCl: 100 mM NaCl, [in 10 mM HEPES (pH 7.5), 1 mM EDTA]
KCl: 20 mM KCl [in 20 mM Tris (pH 8.5), 1 mM EDTA]
[c]With primer-template T in KCl, the K_D value was determined three times. Experiments with the single-stranded U DNA in NaCl and all experiments with V93Q were also performed in triplicate. The average ± the standard deviation is given. Other K_D values were measured once only.
[d]Exo$^-$ variants contained the additional mutation D215A (28).
ND = not determined.

The gain in affinity can be accounted for by a reduction in ionic strength; 20 mM KCl in this investigation and 100 mM NaCl in the earlier study. Protein–DNA interactions are well known to diminish with increasing salt concentration (33). M247 and Y2161 were changed to alanine to probe their potential roles in primer-template strand separation (Figure 1A and B). Both single mutants and the double variant M247A/Y261A displayed similar affinities for the control primer-template as the wild-type enzyme (Figure 2A and Table 2). *Pfu*-Pol V93Q, a mutant largely disabled in uracil recognition (2,5), was observed to bind all primer-templates (T, U+2 and U+4), with K_D values of ~30–40 nM (Table 2 and Supplementary Figure S1). The dissociation constants shown in Table 2 suggest that polymerase (wild type, M247A, Y261A and V93Q) levels of ~0.5 μM should lead to complete primer-template binding.

It is also critical to demonstrate that M247A and Y261A do not compromise uracil recognition. In the low-ionic-strength KCl buffer, the U+2 and U+4 primer-templates were bound more tightly than the control DNA substrates, and the observed sub-nanomolar K_D values could not be accurately determined at the 1 nM concentration of HEX-labelled DNA used (34). Therefore, a second set of experiments was carried out with a 100 mM NaCl buffer, previously used for investigating *Pfu*-Pol (2–5). As anticipated, the increased ionic strength allowed determination of K_D values for binding of the U+2/U+4 primer-templates. Each mutant behaved identically to the wild type, with dissociation constants of ~3.5 nM and 0.5 nM for U+2 and U+4, respectively (Table 2). The 5-fold preferential binding of U+4 agrees with previous data (3). Disabling the proof-reading exonuclease activity (D215A) had no influence on K_D. Interaction with uracil was further probed using

uracil-containing single-stranded DNA, and the K_D values found in the 100 mM NaCl buffer are summarized in Table 2. The wild type and mutants again gave indistinguishable results, and K_D values (just less than 5 nM) agree reasonably with published data (3,4). Using single-stranded uracil DNA in the KCl buffer gave K_D values slightly less than 1 nM for all *Pfu*-Pol variants (Figure 2B and Table 2).

Steady-state fluorescence of free and polymerase-bound AP primer-templates

The primer-templates used in this study (Table 1) have AP positioned next to the terminal 3′ base of the primer, anticipated to maximize stacking interactions owing to the presence of two flanking bases. Therefore, AP fluorescence was, as expected, very low for the free primer-templates, all of which (T, U+2 and U+4) demonstrated near-identical emission spectra with a maximum around 368 nm (Supplementary Figure S2). Spectra were barely altered by addition or Ca^{2+} and Mg^{2+}. Subsequent experiments measured the AP fluorescence of polymerase-bound primer-templates using protein concentrations of 8 μM and DNA levels of 2 μM. This protein concentration is 20-fold greater than the highest K_D (~40 nM found with T-containing control primer-templates and V93Q, Table 2), ensuring virtually complete binding of DNA, with only traces expected to remain free is solution.

AP spectra of primer-templates in complex with *Pfu*-Pol (exo^+) could be measured providing contaminating divalent metal ions were removed from buffers, enzyme and DNA stocks using Chelex resin. With these precautions, spectra did not show any increase in fluorescence over time in the absence of added metal or with 2 mM Ca^{2+}, an inert surrogate that does not support exonuclease activity (35,36) (Supplementary Figure S3). Omitting the Chelex treatment resulted in a time-dependent increase in AP fluorescence, arising from the release of strongly fluorescent free AP owing to traces of metal activating the 3′–5′ proof-reading exonuclease. As expected, addition of Mg^{2+}, an essential co-factor for exonuclease activity (10,13), resulted in liberation of AP and a time-dependent increase in fluorescence (Supplementary Figure S3).

On addition of *Pfu*-Pol (exo^+) to the primer-templates shown in Table 1, the AP fluorescence observed with U+2 increased markedly, suggesting that AP becomes located in a less stacked environment. A noticeably smaller fluorescence enhancement was seen with both T (control) and U+4, implying less pronounced perturbation of DNA structure (Figure 3A). When Ca^{2+} was added, a small enhancement in fluorescence was seen with all three primer-templates, although the position of the emission maxima, just below 370 nm, did not change. As expected, investigation was not possible with *Pfu*-Pol (exo^+) in the presence of Mg^{2+}, owing to degradation of the primer. To assess any influence of this metal ion, AP fluorescence was measured using *Pfu*-Pol D215A, a proof-reading exonuclease–deficient mutant (28). These experiments were carried out using only the primer-templates with deaminated bases at +2 and +4, and in general, the spectra observed were similar to those seen with *Pfu*-Pol (exo^+). Thus, with *Pfu*-Pol (exo^-), the AP fluorescence of enzyme-bound U+2 DNA was significantly greater than that of U+4, and addition of Ca^{2+} and Mg^{2+} caused a slight increase in intensity, with the two metals behaving similarly (Figure 3B). One slight difference was observed between exonuclease-proficient and -deficient enzymes, a small shift in the emission maximum with U+2: ~368 nm for exo^+ and ~372 nm for exo^-. The spectra shown in Figure 3A and B suggest more unwinding and adoption of single-stranded characteristics with U+2 as compared with U+4, results in agreement with structural data showing unwinding of two primer bases with a deaminated base at +2 (which would locate AP in a single strand) and no comparable distortion with U+4 (i.e. retaining AP in a double-stranded environment) (5,8). The augmentation of AP fluorescence seen with U+2 was dependent on interaction of uracil with its specific binding pocket in the N-terminal domain. Use of V93Q, a mutant largely unable to interact with uracil (2,5), resulted in loss of the strong fluorescence enhancement seen with U+2 and the wild-type enzyme; rather, the three primer-templates (T, U+2 and U+4) all gave a similar small fluorescence increase (Figure 3C).

A few studies were carried out with AP at the extreme 3′ end of the primer (data not shown), and similar results were found to those described earlier in the text for internal AP, i.e. more pronounced fluorescence enhancement on binding U+2 as compared with U+4 or T. However, the free primer-templates had higher starting fluorescence (owing to AP lacking a 3′ stacking base), and any fluorescence enhancement after polymerase binding was, therefore, less prominent. In contrast, investigations with T4 polymerase showed that AP at the extreme 3′ end of the primer gave more pronounced fluorescence enhancement than AP one base in from the terminus (21).

Time-resolved fluorescence of free and polymerase-bound AP primer-templates

To further clarify the DNA transitions that follow the binding of uracil-containing primer-templates, use has been made of time-resolved fluorescence. The AP fluorescence decay function is an excellent reporter of local environment, and in favourable instances, can provide specific structural information, e.g. monitoring base flipping by DNA methyltransferases (25,26) and primer-template dynamics in viral family-B DNA polymerases (15,37).

The decay parameters for free U+2 and U+4 primer-templates were essentially identical and barely changed by the addition of Ca^{2+} or Mg^{2+} (Table 3). Four lifetime (τ) components, commonly observed for AP in DNA (19,25,26), were required to give a satisfactory fit, revealing the existence of at least four conformational populations. The A factors indicate the fractional population of individual conformational states. One has a very short lifetime of ~0.05 ns (τ_1) and accounts for ~80% of the duplex population (A_1). This corresponds to a highly stacked structure in which excited AP is

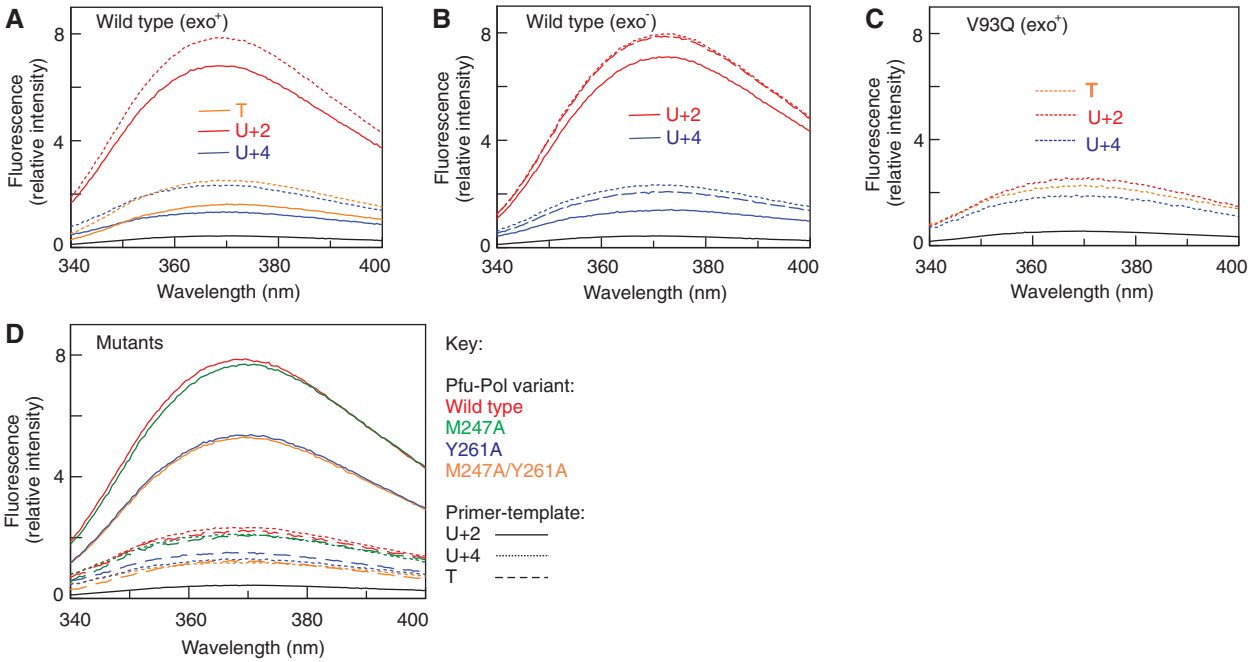

Figure 3. AP fluorescence emission spectra of primer-templates (U+2, U+4 and a T-containing control) bound to *Pfu*-Pol B. (**A**) Spectra observed in the presence of *Pfu*-Pol exo$^+$. The three primer-templates (full sequences given in Table 1) are distinguished by colour coding. The solid lines are the spectra observed in the absence of divalent metals, and the dotted lines in the presence of 2 mM $CaCl_2$. (**B**) Spectra seen with *Pfu*-Pol exo$^-$ (D215A). Colour coding is used to distinguish U+2 and U+4. The solid, dotted and hatched lines represent, respectively, the spectra measured without metal ions and with 2 mM $CaCl_2$ and 2 mM $MgCl_2$. (**C**) Spectra observed with *Pfu*-Pol V93Q (a mutation that disables uracil binding) exo$^+$. The three primer-templates are distinguished by the same colour coding used in panel (A), and these spectra were all recorded in the presence of 2 mM $CaCl_2$. (**D**) Spectra measured with M247A, Y261A and the double mutant M247A/Y261A (wild type included for comparison). *Pfu*-Pol variants are identified by the colour coding shown in the key to the right of the panel. Three spectra were recorded, with each protein bound to primer-templates containing U+2, U+4 and T (control). The different primer-templates are distinguished using solid, hatched and dotted lines as described in the key. These spectra were recorded with exo$^+$ variants in the presence of 2 mM $CaCl_2$. All the spectra shown in panels A–D used an excitation wavelength of 315 nm,with DNA and polymerase concentrations of 2 and 8 μM, respectively. The black line of low intensity represents the spectrum of a free primer-template, included for comparative purposes.

Table 3. Fluorescence lifetimes (τ_i) and their fractional amplitudes (A_i) for the AP-containing primers U+2 and U+4 (see Table 1)

Solution composition	τ_1/ns	τ_2/ns	τ_3/ns	τ_4/ns	A_1	A_2	A_3	A_4
U+2	0.05	0.51	2.5	8.2	0.78	0.13	0.07	0.03
U+2/Ca^{2+}	0.05	0.54	2.6	8.4	0.77	0.13	0.07	0.03
U+2/Mg^{2+}	0.05	0.55	2.8	9.2	0.79	0.12	0.06	0.03
U+4	0.05	0.50	2.6	8.4	0.77	0.13	0.07	0.03
U+4/Ca^{2+}	0.05	0.52	2.7	8.5	0.77	0.13	0.07	0.03
U+4/Mg^{2+}	0.04	0.53	2.7	9.0	0.80	0.11	0.06	0.02
U+2/*Pfu*-Pol (exo$^+$)	0.20	1.0	3.8	8.2	0.35	0.24	0.27	0.15
U+2/*Pfu*-Pol (exo$^+$)/Ca^{2+}	0.17	0.99	3.7	8.1	0.28	0.23	0.30	0.19
U+4/*Pfu*-Pol (exo$^+$)	0.08	0.90	3.0	8.3	0.55	0.24	0.16	0.04
U+4/*Pfu*-Pol (exo$^-$)/Ca^{2+}	0.09	1.0	3.5	9.6	0.50	0.26	0.17	0.06
U+2/*Pfu*-Pol (exo$^-$)/Ca^{2+}	0.17	0.94	3.6	9.0	0.42	0.29	0.19	0.10
U+2/*Pfu*-Pol (exo$^-$)/Mg^{2+}	0.17	0.99	3.7	8.7	0.40	0.23	0.23	0.14
U+4/*Pfu*-Pol (exo$^-$)/Ca^{2+}	0.06	0.67	3.6	9.5	0.64	0.12	0.15	0.09
U+4/*Pfu*-Pol (exo$^-$)/Mg^{2+}	0.06	0.67	3.5	9.4	0.66	0.11	0.15	0.08

rapidly quenched by interaction with neighbouring bases. The longest decay time (8–9 ns) is similar to that of free AP-riboside (38) and is attributed to AP in an extrahelical environment, free from interbase quenching. This species constitutes a very small fraction of the total population, ~3%. The two intermediate decay times, accounting for ~20% of duplexes, are due to imperfectly stacked conformations in which AP is intrahelical, but quenching is much less efficient than in the closely stacked structure.

Substantial changes were observed when *Pfu*-Pol exo$^+$ was added to U+2 (Figure 4A and Table 3). The three shortest lifetimes (τ_1, τ_2 and τ_3) increased, indicating a

loss of quenching and a change in local environment. Of particular significance are the large increase in τ_1 to 0.2 ns and the considerable decrease in A_1 to 35%. The greater value of τ_1 indicates a smaller degree of stacking in this conformational state, and the decrease in A_1 (and concomitant increases in A_2–A_4) shows a large transfer of duplex population to more poorly stacked states. These effects are consistent with unwinding of the duplex seen structurally with primer-templates containing hypoxanthine at +2 (8). When Ca^{2+} was present, even less of the most highly stacked conformation was seen, with A_1 reduced to 28%. Much less perturbation was observed for U+4 in complex with the exo$^+$ polymerase. Noticeably, the effect on the shortest decay component, highly stacked AP, was markedly different than for U+2. The shortest decay time increases to 0.08/0.09 ns, much less than 0.17/0.20 ns seen with U+2, and 50–55% of the population persists in this conformation (cf. 28–35% with U+2). The values of τ_2, τ_3 and τ_4 are similar in both complexes, indicating that AP in less stacked or extrahelical states experiences a similar environment in both cases, as might be expected. Overall, the decay parameters for U+4 bound to the polymerase indicate a modest distortion of the duplex, resulting in some transfer from the best stacked conformations (τ_1) to poorly stacked or extrahelical states, but with ~50% (A_1) remaining in the well-stacked state. Again, these data agree with a polymerase–U+4 structure, where no major changes in the duplex region of the primer-template are observed (5).

Experiments were also carried out with *Pfu*-Pol exo$^-$ (Figure 4B and Table 3), and in general, the fluorescence lifetime parameters follow the trends discussed earlier in the text for exo$^+$, confirming that greater DNA distortion occurs with U+2 than U+4. This is most clearly illustrated by the parameters for the most highly stacked state; thus, the τ_1 lifetime is longer for U+2 (0.17 ns) than U+4 (0.06 ns), and the occupancy of this state is less for U+2 (40–42%) than U+4 (64–66%). These spectra were recorded with either Ca^{2+} or Mg^{2+}, which behaved similarly, suggesting the two metals influence the protein–DNA interaction in a near-identical manner. Close comparison of the decay parameters for exo$^-$ (Figure 4B) with those of exo$^+$ (Table 3) shows that the exo$^-$ variant induces somewhat less distortion of the U+2 primer-template. Higher occupancy (40–42%) of the best-stacked state persists in the exo$^-$ U+2 complex (with Ca^{2+} or Mg^{2+}), a value reduced to 28% for the analogous complex with exo$^+$. Although both the proof-reading–proficient and –deficient *Pfu*-Pol variants can unwind U+2-containing primer-templates, exo$^+$ seems slightly more potent.

Exonucleolysis of AP-containing primer-templates

Previous results from our group showed that U+2 primer-templates are more susceptible to proof reading by *Pfu*-Pol than U+4 (7). However, the increase in exonuclease activity with U+2, relative to U+4, depended on the base pairs in the double-stranded region adjacent to the primer-template junction. When the last two base pairs were both G:C, a stimulation (ratio of the exonuclease rates: U+2/U+4) of just more than 200 was observed. With two A:T base pairs, this factor was reduced to just more than 100 (7). The fluorescence results described earlier in the text with the AP-containing primer-templates suggest unwinding in the case of U+2 but not U+4. Therefore, a faster rate of exonucleolytic degradation of the U+2 primer, compared with U+4, is anticipated. However, the duplex regions of both primer-templates terminate with an AP:T followed by an A:T base pair (Table 1). AP:T base pairs are marginally less stable than A:T (39), and in view of the influence of base pair stability on exonuclease rates, it was decided to confirm the degradation of the primer-templates listed in Table 1.

Figure 5 shows the results obtained when U+2, U+4 and a control primer-template (T) lacking uracil were subject to proof-reading exonucleolysis by *Pfu*-Pol. The low-ionic-strength Tris–KCl buffer was used, such that the protein concentration (500 nM) was in excess of DNA (10 nM) and sufficiently more than the weakest K_D (32 nM for the T primer-template) (Table 2), to

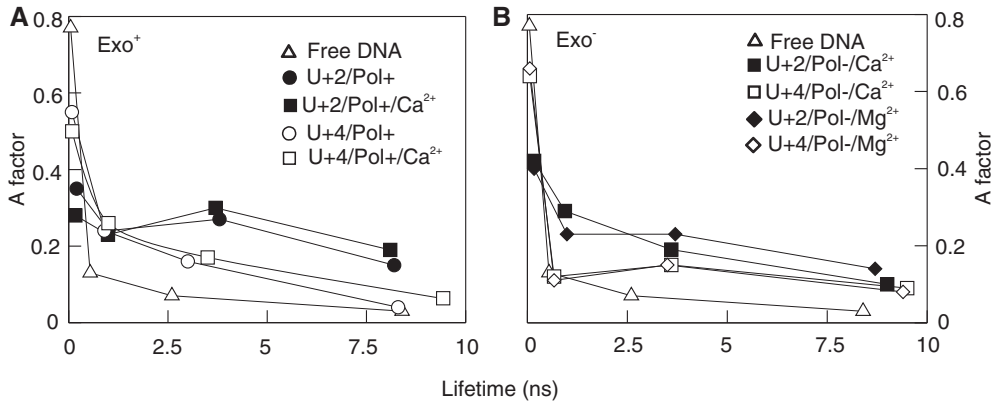

Figure 4. Graphical representation of the AP fluorescence decay parameters [fractional amplitude (A factor) versus lifetime (τ)] for uracil-containing primer-templates. (**A**) Parameters observed with *Pfu*-Pol exo$^+$ bound to U+2 and U+4 in the presence and absence of Ca^{2+}. (**B**) Parameters observed with *Pfu*-Pol exo$^-$ (D215A) bound to U+2 and U+4 in the presence of Ca^{2+} and Mg^{2+}. For both A and B, the excitation wavelength was 315 nm, and the concentrations of primer-template and *Pfu*-Pol were 2 μM and 8 μM, respectively. The free DNA trace given is that found for U+2 in the presence of Ca^{2+}, but all free primer-templates showed near-identical parameters (Table 3).

ensure full binding of the DNA. In contrast to earlier studies, the addition of PCNA was, therefore, not required to guarantee complete saturation (7). The degradation patterns were analysed by gel electrophoresis (Figure 5A–C), and the amount of starting material remaining at various times (intensity of starting material band/sum of the intensity of all bands) was determined. This data were used to generate plots of starting material remaining versus time (Figure 5D and E) and, subsequently, to determine the rate constant associated with the disappearance of starting material for each reaction (Table 3). The AP primer-template with U at the +2 position is hydrolysed 14-fold more rapidly than U+4 (Table 4), an enhancement less than seen previously for DNA with standard base pairs near the primer-template junction (7). However, the results seen here continue the trend that 'weaker' base pairs lead to a less profound difference in the rates at which U+2 and U+4 primer-templates are degraded. The control primer-template (T), lacking uracil, is degraded at a rate intermediate between U+2 and U+4 (Table 4), similar to previous observations (7).

Investigation of the roles of arginine 247 and tyrosine 261 in primer-strand unwinding

As discussed in the introduction, and shown in Figure 1A and B, structural studies appeared to show that R247 and Y261 play an important role in primer-template strand separation. The equivalent amino acids in *Pfu*-Pol, M247 and Y261 were individually changed to alanine to probe their functions. A double mutation, in which both amino acids were altered to alanine, was also prepared. The influence of the three mutations on the steady-state fluorescence of the AP-containing DNA was determined. These experiments were carried out with *Pfu*-Pol (exo^+) in the presence of the non-activating metal Ca^{2+}, representing the nearest inactive mimic of the exonuclease-proficient polymerase-DNA-Mg^{2+} ternary complex. Binding to the U+2 primer-template, by all three mutant polymerases (M247A, Y261A and M247A/Y261A), gives rise to greater enhancement of AP fluorescence than seen with U+4 or the T control, with the latter pair giving roughly the same small increase (Figure 3D). M247A behaves in an identical manner to the wild-type enzyme, with both polymerases producing nearly superimposable spectra with all three primer-templates and, consequently, matching increases in AP fluorescence on binding U+2. In contrast, the fluorescent enhancement seen with Y261A, with all three primer-templates, is less than that observed with the wild type: by ~30% for U+2 and 45% for U+4 and T (although the latter two are difficult to determine accurately owing to low fluorescence intensities). These results suggest that amino acid Y261 plays a general role in unwinding primer-templates or maintaining strand separation during the switch from polymerization to exonuclease mode that precedes proof-reading activity. The spectra

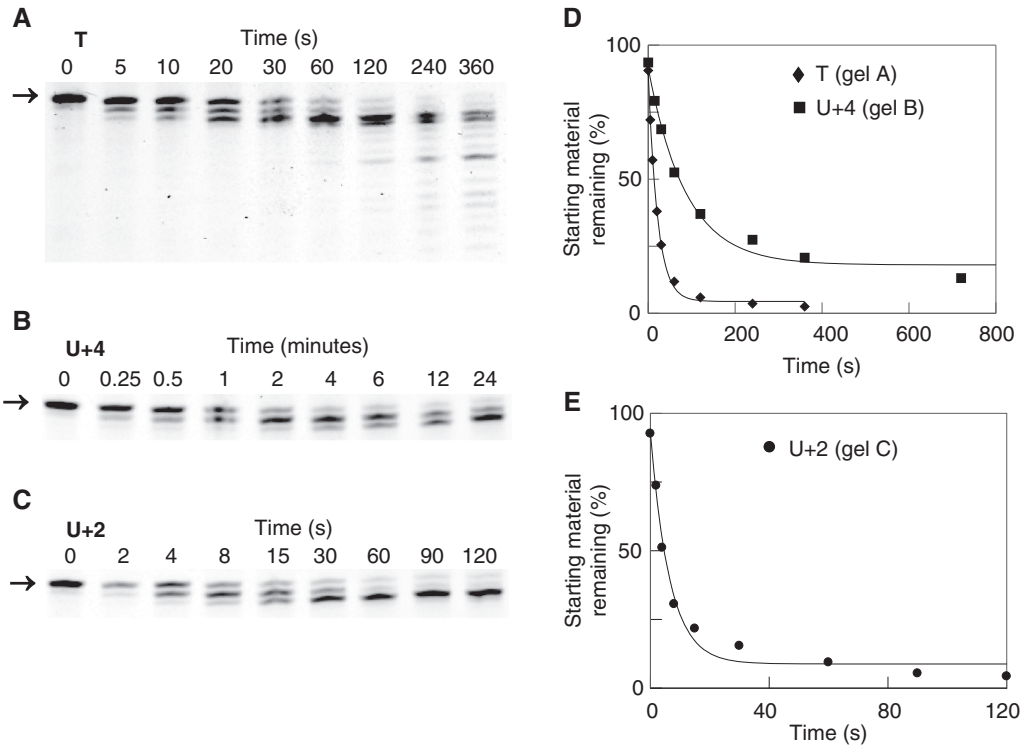

Figure 5. Hydrolysis of AP-containing primer-templates by the proof-reading exonuclease activity of wild-type *Pfu*-Pol B. (**A**) T primer-template; (**B**) U+4 primer-template; (**C**) U+2 primer-template. Panels A–C show the degradation of the 6-FAM–labelled primer strand (starting material show by the arrows) with time, as assessed using gel electrophoresis. Where gels have been cropped, no smaller degradation products were visible. (**D** and **E**) Fits of the data obtained in panels A–C (key to lines given in graph) to a single exponential decay to obtain the rate constants summarized in Table 4.

Table 4. Rates of 3′–5′ proof-reading exonuclease activity seen with *Pfu*-Pol B (wild type and mutants) and the DNA substrates given in Table 1

Primer-template[a]	Exonucleolysis rate constants (min^{-1}) of *Pfu*-Pol variants[b]		
	Wild type	M247A	Y261A
T	2.7 ± 0.1	2.8 ± 0.04	1.2 ± 0.04
U+2	9.9 ± 0.9	9.9 ± 2.0	9.8 ± 0.6
U+4	0.7 ± 0.1	0.6 ± 0.1	0.2 ± 0.06

[a]The DNA substrates used are listed in Table 1.
[b]Rates ± standard deviation from at least three observations.

Table 5. Error rates of *Pfu*-Pol B variants determined using pSJ2[a]

Polymerase	Number of colonies[b]	Number of mutant (white) colonies	Corrected mutation frequency[c]	Error rate[d]
Wild type (exo^+)[e]	25 700	11	3.2×10^{-4}	1.6×10^{-6}
M247A (exo^+)	34 783	16	3.5×10^{-4}	1.7×10^{-6}
Y261A (exo^+)	15 429	14	8.0×10^{-4}	4.0×10^{-6}

[a]For full details, see (32).
[b]Sum of three independent experiments, each consisting of five repeats.
[c]The mutation frequency is the ratio of white colonies to total colonies. The values given have been corrected by subtracting the background mutation frequency of 1.1×10^{-4} observed for gapped pSJ2 (32).
[d]The error rate is the incidence at which the polymerase incorporates incorrect dNTPs per templating base. For full details of how the mutation frequency is used to derive the error rate, see (32).
[e]Taken from (32).

seen with the double mutant M247A/Y261A are almost identical to those observed for Y261A alone and can be simply accounted for by the change at amino acid 261.

The steady-state fluorescence data seen with the mutant polymerases have been complemented by determining the rate constants for proof-reading exonuclease activity (Supplementary Figure S4 and Table 4). With all primer-templates (U+2, U+4 and T control), changing methionine 247 to alanine has very little influence on hydrolysis rates, which were almost identical to those seen with the wild-type polymerase. With Y261A, a noticeable drop in the rate constants for exonuclease activity (~2- to 3-fold) was noticed with the U+4 and T substrates. However, with U+2, Y261A and the wild type showed similar activity. Finally, an *in vitro* DNA polymerase fidelity assay (32) has been used to measure the accuracy with which the mutants incorporate dNTPs. As summarized in Table 5, the wild type and M247A have similar error rates of $\sim 1.6 \times 10^{-6}$. Y261A has noticeably lower fidelity, with an error rate of $\sim 4 \times 10^{-6}$, ~2.5-fold more error prone than the wild type.

CONCLUSIONS

This publication uses steady-state and time-resolved fluorescence of AP-containing DNA to demonstrate pronounced primer-template separation when uracil is encountered at the +2 position by archaeal family-B DNA polymerases. Both techniques show an increase in AP fluorescence on protein binding, consistent with diminished stacking of the modified base as it moves from a double- to a single-stranded environment (Figures 3 and 4 and Table 3). The fluorescence decay parameters provide convincing evidence for a decrease in the amount of double-stranded DNA, manifested by marked weakening of interbase stacking (as indicated by the increase in the lifetime of the shortest-lifetime component, τ_1) and a large transfer of population from highly stacked to poorly stacked conformations. The fluorescence data found with the U+2 primer-template, inferring strand separation, agree with structural studies (8). In contrast, a smaller increase in AP fluorescence intensity with only a slight increase in the lifetime of the shortest component (τ_1), together with the persistence of a high population of strongly stacked states, is seen with U+4 (and T control) primer-template-enzyme complexes, suggesting less profound DNA distortion, again in agreement with X-ray crystallography (5). Kinetic measurements showed the AP-containing U+2 primer-template to be more susceptible to proof-reading exonuclease activity than U+4. DNA unwinding is a pre-requisite for proof reading (9,13), indicating that the degree of strand separation seen with U+2 and U+4 correlates with the rate at which they are subject to exonucleolysis.

Many steady-state and time-resolved measurements have been carried out with T4 and RB69 polymerases using AP-containing DNA (15,20,21,37), but exact comparison with *Pfu*-Pol is not straightforward. All polymerases belong to the B family and possess obvious sequence and structural homology, even though the viral enzymes do not interact with uracil (2). Studies with the viral polymerases used primers containing AP at the extreme 3′ end, a different location to that used here, and time-resolved experiments (incapable of resolving lifetimes <100 ps) were fitted to three, rather than four, decay components (15,20,21,34). With T4 polymerase, stronger fluorescence enhancement was seen with AP at the primer terminus compared with the −1 location (21), observations that are reversed with *Pfu*-Pol. For the viral enzyme, an aromatic amino acid intercalates between the two penultimate primer bases and has been suggested as the cause of the fluorescence increase with terminal AP (21). Archaeal enzymes lack an equivalent intercalating amino acid (5,8), suggesting subtle differences in the mechanism used for strand separation. In the case of T4 and RB69 polymerases, more pronounced AP fluorescence enhancement was seen with proof-reading exonuclease–proficient variants (15,20), whereas *Pfu*-Pol exo^+ and exo^- gave similar increases. In general, binding of viral polymerases enhances the steady-state fluorescence of AP primer-templates, and time-resolved experiments demonstrate a reduction in the population of shorter-lifetime components (15,20,21,37), interpreted as evidence for increased strand separation on formation of exonuclease-competent complexes. The conclusions drawn with viral polymerases agree with the proposal

that U+2 primer-templates undergo greater strand separation than U+4 (and control primer-templates), after *Pfu*-Pol binding.

Proof reading normally takes place after dNMP misincorporation, the resulting mismatched base pair being prone to unwinding, thus favouring strand separation that necessarily precedes exonucleolysis (13). No mismatched base pairs are present during uracil recognition, requiring unravelling of a fully Watson–Crick base-paired primer-template to initiate proof-reading activity. To elucidate features contributing to the unwinding of a stable duplex, attention has focussed on two amino acids, suggested to be important by structural studies (8). The amino acid at position 247 (arginine in *Tgo*-Pol, methionine in *Pfu*-Pol) is at the tip of the β-hairpin, a structural element implicated in primer-template strand separation (12–16). R247 stacks against one of the single-stranded template bases that arise after partial primer-template denaturation (Figure 1B) and may act as a wedge to pry apart the strands (8). A second amino acid, tyrosine 261, is located on an α-helix and positioned between separated primer and template bases (Figure 1B), possibly preventing re-annealing (8). Both M247 and Y261 have been converted to alanine, and a double mutant has also been prepared. In steady-state AP fluorescence, M247A showed almost identical properties to the wild type (Figure 3D). In contrast, Y261A resulted in a smaller increase in AP fluorescence with all three primer-templates (Figure 3D). The double mutant behaved almost identically to Y261A and was not investigated further. The proof-reading activity of M247A was indistinguishable from the wild-type enzyme; with Y261A, a drop in rate was observed with the T control and U+4, but not with U+2 (Table 4). It is concluded that M247 plays no role in strand separation and proof reading during uracil recognition. Most likely the long side chain of amino acid 247 is flexible and the position of R247 in the structure of *Tgo*-Pol (Figure 1A and B) (5) is fortuitous, misleadingly implying an important function. A recent structure of an RB69 repair complex has indicated that R260 (the corresponding amino acid) does not contact either the primer or template strand (40). In contrast, Y261 plays an important role, with its removal leading to less strand separation and, with the T control and U+4, slower proof reading. As primer-template unwinding appears to be the rate-limiting step for proof reading (13), it follows that altering an amino acid that plays an important role in this process should reduce 3′–5’ exonucleolysis. With U+2, strand separation is highly favoured and may no longer be rate limiting in the overall proof-reading cycle. Such a change in the rate-limiting step may account for Y261A degrading the U+2 primer-template at the same rate as the wild-type enzyme. Confirmation of the different behaviours of M247 and Y261 comes from an *in vitro* fidelity assay. M247A is as accurate as the wild type, while Y261A makes 2.5 times as many mistakes (Table 5). This experiment is conceptually similar to *in vivo* fidelity determination, used to investigate proof reading in viral polymerases (13,41).

Further information about the significance of *Pfu*-Pol M247 and Y261 is available from sequence comparisons. The β-hairpin amino acid at position 247 does not show pronounced retention even within the thermococcales order, and when the wider euryarchaeotal phylum is considered, no conservation can be discerned (Table 6). It is difficult to see how the small amino acids, often found naturally at this position (equivalent to the alanine mutation), could fulfil the wedge function previously proposed for the separation of primer-template strands (5). As mentioned previously, the equivalent amino acid in RB69 polymerase (R260) appears to be unimportant; rather, two alternative β-hairpin amino acids, M256 and Y257, are sandwiched between the primer and template and appear to play a key role in strand separation (40). Similarly the analogue of *Pfu*-Pol M247 observed in T4 polymerase (K257) can be changed to several amino acids with little change in fidelity (15). The observation that the β-hairpin tends to show conservation at the structural level, rather than in amino acid sequence, (13,14) may be critical. The motif may act as a whole to partition primer and template strands; therefore, changes to particular amino acids, such as to the amino acid at position 247 in archaeal polymerase B, may have marginal influence. Much higher conservation is seen with the α-helix–located amino acid at position 261 (Table 6). Considering the euryarchaea as a whole, this amino acid is invariably an aromatic or a large aliphatic entity. The proposed role of amino acid 261 in keeping apart separated primer-template strands could easily be fulfilled by any of these large hydrophobic side chains. The nature of this amino acid is retained for almost all family-B polymerases (data not shown). With the well-characterized polymerases from phages RB69 and T4, the equivalent amino acids are Ile 274 and Leu 271, respectively. RB69 Ile 274 shows pronounced spatial overlap with *Tgo*-Pol Y261, both at the amino acid and α-helix secondary structure level (Figure 1C). Several RB69 DNA structures show that Ile 274 is near the separation point of the primer and template strands (12,41,42). With T4 polymerase, insertion of an additional leucine adjacent to Leu 271 decreases fidelity, indicating a role for this region (13,43). However, as the change is not a direct substitution of Leu 271, it is difficult to decipher the role of the amino acid itself.

In summary, this publication has used AP fluorescence to demonstrate that archaeal DNA polymerases denature primer-templates and initiate proof reading as they

Table 6. Identity of amino acids at position 247 and 261 in euryarchaeal family-B DNA polymerases

Species	Amino acid 247	Amino acid 261
Thermococcales (33 members)	R19, S7, M6, G1	Y25, F8
Euryarchaea (minus thermococcales) (78 members)	N12, A10, F9, Q9, R8, I7, E5, G4, L4, V4, H2, K1, S1, L1, M1	Y42, L23, W7, F5, V1

approach template-strand uracil. Tyrosine 261 has been shown to contribute to DNA unwinding and fidelity, although its influence is not specific for uracil recognition, and rather, the amino acid acts generally with all primer-templates. The capture of uracil by the deaminated base–binding pocket is, almost certainly, the source of binding energy used to unwind the fully complementary primer-template (7). Overall, the enzyme performs a remarkable job in proof reading, rather than extending, a fully Watson–Crick base-paired primer-template, preventing copying of template-strand uracil and the transmission of fixed mutations to progeny.

SUPPLEMENTARY DATA

Supplementary Data are available at NAR Online: Supplementary Figures 1–4.

ACKNOWLEDGEMENTS

Jochen Arlt is thanked for skilled technical assistance. The advice and comments of Dr. David Dryden (Department of Chemistry, University of Edinburgh) were highly appreciated. Dr. Susan Firbank is thanked for preparing Figure 1.

FUNDING

T.T.R. and B.J.K. were UK-BBSRC supported PhD students and X.W. was supported by an EaStCHEM PhD scholarship. Work at Newcastle was supported by the UK BBSRC (BB/F015895/1) and the Wellcome Trust (064345). Funding for open access charge: UK Wellcome Trust.

Conflict of interest statement. None declared.

REFERENCES

1. Greagg,M.A., Fogg,M.J., Panayotou,G., Evans,S.J., Connolly,B.A. and Pearl,L.H. (1999) A read-ahead function in archaeal DNA polymerases detects pro-mutagenic template-strand uracil. *Proc. Natl Acad. Sci. USA*, **96**, 9045–9050.
2. Fogg,M.J., Pearl,L.H. and Connolly,B.A. (2002) Structural basis for uracil recognition by archaeal family B DNA polymerases. *Nat. Struct. Biol.*, **9**, 922–927.
3. Shuttleworth,G., Fogg,M.J., Kurpiewski,M.R., Jen-Jacobson,L. and Connolly,B.A. (2004) Recognition of the pro-mutagenic base uracil by family B DNA polymerases from archaea. *J. Mol. Biol.*, **337**, 621–634.
4. Gill,S., O'Neill,R., Lewis,R.J. and Connolly,B.A. (2007) Interaction of the family-B DNA polymerase from the archaeon *Pyrococcus furiosus* with deaminated bases. *J. Mol. Biol.*, **372**, 855–863.
5. Firbank,S.J., Wardle,J., Heslop,P., Lewis,R.J. and Connolly,B.A. (2008) Uracil recognition in archaeal DNA polymerases captured by X-ray crystallography. *J. Mol. Biol.*, **381**, 529–539.
6. Connolly,B.A. (2009) Recognition of deaminated bases by archaeal family-B DNA polymerases. *Biochem. Soc. Trans.*, **37**, 65–68.
7. Russell,H.J., Richardson,T.T., Emptage,K. and Connolly,B.A. (2009) The 3′–5′ proofreading exonuclease of archaeal family-B DNA polymerase hinders the copying of template strand deaminated bases. *Nucleic Acids Res.*, **37**, 7603–7611.
8. Killelea,T., Ghosh,S., Tan,S.S., Heslop,P., Firbank,S., Kool,E.T. and Connolly,B.A. (2010) Probing the interaction of archaeal DNA polymerases with deaminated bases using X-ray crystallography and non-hydrogen bonding isosteric base analogues. *Biochemistry*, **49**, 5772–5781.
9. Joyce,C.M. (1989) How DNA travels between the separate polymerase and 3′–5′ exonuclease sites of DNA polymerase I (Klenow fragment). *J. Biol. Chem.*, **264**, 10858–10866.
10. Joyce,C.M. and Steitz,T.A. (1994) Function and structure relationships in DNA polymerases. *Annu. Rev. Biochem.*, **63**, 777–822.
11. Brautigam,C.A. and Steitz,T.A. (1998) Structural and functional insights provided by crystal structures of DNA polymerases and their substrate complexes. *Curr. Opin. Struct. Biol.*, **8**, 54–63.
12. Shamoo,Y. and Steitz,T.A. (1999) Building a replisome from interacting pieces: sliding clamp complexed to a peptide from DNA polymerase and a polymerase editing complex. *Cell*, **99**, 155–166.
13. Reha-Krantz,L.J. (2010) DNA polymerase proofreading: Multiple roles maintain genome stability. *Biochim. Biophys. Acta*, **1804**, 1049–1063.
14. Trzenecka,A., Pzochocka,D. and Bebenek,A. (2009) Different behaviors *in vivo* of mutations in the β hairpin loop of the DNA polymerases of the closely related phages T4 and RB69. *J. Mol. Biol.*, **289**, 797–807.
15. Subuddhi,U., Hogg,M. and Reha-Kranz,L.J. (2008) Use of 2-aminopurine fluorescence to study the role of the β hairpin in the proofreading pathway catalyzed by the phage T4 and RB69 DNA polymerases. *Biochemistry*, **47**, 6130–6137.
16. Hogg,M., Aller,P., Konigsberg,W., Wallace,S.S. and Doublie,S. (2007) Structural and biochemical investigation of the role in proofreading of a β hairpin loop found in the exonuclease domain of a replicative DNA polymerase of the B family. *J. Biol. Chem.*, **282**, 1432–1444.
17. Guest,C.R., Hochstrasser,R.A., Sowers,L.C. and Millar,D.P. (1991) Dynamics of mismatched base pairs in DNA. *Biochemistry*, **30**, 3271–3279.
18. Stivers,J.T. (1998) 2-Aminopurine fluorescence studies of base stacking interactions at abasic sites in DNA: metal-ion and base sequence effects. *Nucleic Acids Res.*, **26**, 3837–3844.
19. Jean,J.M. and Hall,K.B. (2001) 2-Aminopurine fluorescence quenching and lifetimes: role of base stacking. *Proc. Natl. Acad. Sci. USA*, **98**, 37–41.
20. Bloom,L.M., Otto,M.R., Eritja,R., Reha-Krantz,L.J., Goodman,M.F. and Beechem,J.M. (1994) Pre-steady-state kinetic analysis of sequence-dependent nucleotide excision by the 3′-exonuclease activity of bacteriophage T4 DNA polymerase. *Biochemistry*, **33**, 7576–7586.
21. Beechem,J.M., Otto,M.R., Bloom,L.B., Eritja,R., Reha-Krantz,L.J. and Goodman,M.F. (1998) Exonuclease-polymerase active site partitioning of primer-template DNA strands and equilibrium Mg^{2+} binding properties of bacteriophage T4 DNA polymerase. *Biochemistry*, **37**, 10144–10155.
22. Bandwar,R.P. and Patel,S.S. (2001) Peculiar 2-aminopurine fluorescence monitors the dynamics of open complex formation by bacteriophage T7 RNA polymerase. *J. Biol. Chem.*, **276**, 14075–14082.
23. Stivers,J.T., Pankiewicz,K.W. and Watanabe,K.A. (1999) Kinetic mechanism of damage site recognition and uracil flipping by *Escherichia coli* uracil DNA glycosylase. *Biochemistry*, **38**, 952–963.
24. Allan,B.W., Reich,N.O. and Beechem,J.M. (1999) Measurement of the absolute temporal coupling between DNA binding and base flipping. *Biochemistry*, **38**, 5308–5314.
25. Neely,R.K., Daujotyte,D., Grazulis,S., Magennis,S.W., Dryden,D.T.F., Klimasauskas,S. and Jones,A.C. (2005) Time-resolved fluorescence of 2-aminopurine as a probe of base flipping in M.HhaI–DNA complexes. *Nucleic Acids Res.*, **33**, 6953–6960.
26. Youngblood,B., Bonnist,E., Dryden,D.T.F., Jones,A.C. and Reich,N.O. (2008) Differential stabilization of reaction intermediates: specificity checkpoints for M.EcoRI revealed by transient fluorescence and fluorescence lifetime studies. *Nucleic Acids Res.*, **36**, 2917–2925.

27. McCullough,A.K., Dodson,M.L., Scharer,O.D. and Lloyd,R.S. (1997) The role of base flipping in damage recognition and catalysis by T4 endonuclease V. *J. Biol. Chem.*, **272**, 27210–27217.
28. Evans,S.J., Fogg,M.J., Mamone,A., Davis,M., Pearl,L.H. and Connolly,B.A. (2000) Improving dideoxynucleotide-triphosphate utilization by the hyper-thermophilic DNA polymerase from Pyrococcus furiosus. *Nucleic Acids Res.*, **28**, 1059–1066.
29. Emptage,K., O'Neill,R., Solovyova,A. and Connolly,B.A. (2008) Interplay between DNA polymerase and proliferating cell nuclear antigen switches off base excision repair of uracil and hypoxanthine during replication in archaea. *J. Mol. Biol.*, **383**, 762–771.
30. Connolly,B.A. (1991) Oligodeoxynucleotides contained modified bases. In: Eckstein,F. (ed.), *Oligonucleotides and Analogues, a Practical Approach*. Oxford University Press, Oxford, pp. 155–183.
31. Connolly,B.A. (1992) Synthetic oligodeoxynucleotides containing modified bases. *Methods Enzymol.*, **211**, 36–53.
32. Keith,B.J., Jozwiakowski,S.K. and Connolly,B.A. (2013) A plasmid-based *lacZα* gene assay for DNA polymerase fidelity measurement. *Anal. Biochem*, **433**, 153–161.
33. Record,M.T., Lohman,T.M. and De Haseth,P. (1976) Ion effects on ligand-nucleic acid interactions. *J. Mol. Biol.*, **107**, 145–158.
34. Reid,S.L., Parry,D., Hsiao-Hui,L. and Connolly,B.A. (2001) Binding and recognition of GATATC target sequences by the EcoRV restriction endonuclease: a study using fluorescent oligonucleotides and fluorescence polarisation. *Biochemistry*, **40**, 2484–2494.
35. Beese,L.S. and Steitz,T.A. (1991) Structural basis for the 3′–5′ exonuclease activity of Escherichia coli DNA polymerase I: a two metal ion mechanism. *EMBO J.*, **10**, 25–33.
36. Datta,K., Johnson,N.P., LiCata,V.J. and von Hippel,P.H. (2009) Local conformations and competitive binding affinities of single- and double-stranded primer-template DNA at the polymerization and editing active sites of DNA polymerases. *J. Biol. Chem.*, **284**, 17180–17193.
37. Hariharan,C. and Reha-Krantz,L.J. (2005) Using 2-aminopurine fluorescence to detect bacteriophage T4 DNA polymerase-DNA complexes that are important for primer extension and proofreading reactions. *Biochemistry*, **44**, 15674–15684.
38. Neely,R.K., Magennis,S.W., Dryden,D.T.F. and Jones,A.C. (2004) Evidence of tautomerism in 2-aminopurine from fluorescence lifetime measurements. *J. Phys. Chem. B*, **108**, 17606–17610.
39. Law,S.M., Eritja,R., Goodman,M.F. and Breslauer,K.J. (1996) Spectroscopic and calorimetric characterizations of DNA duplexes containing 2-aminopurine. *Biochemistry*, **35**, 12329–12337.
40. Aller,P., Duclos,S., Wallace,S.S. and Doublié,S. (2011) A crystallographic study of the role of sequence context in thymine glycol bypass by a replicative DNA polymerase serendipitously sheds light on the exonuclease complex. *J. Mol. Biol.*, **412**, 22–34.
41. Reha-Krantz,L.J. (1995) Use of genetic analyses to probe structure, function, and dynamics of bacteriophage T4 DNA polymerase. *Methods Enzymol.*, **262**, 323–331.
42. Hogg,M., Wallace,S. and Doublié,S. (2004) Crystallographic snapshots of a replicative DNA polymerase encountering an abasic site. *EMBO J.*, **23**, 1483–1493.
43. Stocki,S.A., Nonay,R.L. and Reha-Krantz,L.J. (1995) Dynamics of bacteriophage T4 DNA polymerase function: identification of amino acid residues that affect switching between polymerase and 3′→5′ exonuclease activities. *J. Mol. Biol.*, **254**, 15–28.